

Electronic Properties of MoS₂/HfO₂ Interface: Impact of Interfacial Impurities during Atomic Layer Deposition Growth

Santosh KC¹, Roberto C. Longo¹, Robert M. Wallace^{1,2} and Kyeongjae Cho^{1,2*}

¹Department of Materials Science & Engineering, The University of Texas at Dallas,
Richardson, Texas 75080, USA

²Department of Physics, The University of Texas at Dallas, Richardson, Texas 75080,
USA

*E-mail: kjcho@utdallas.edu

ABSTRACT

Using *ab-initio* calculations within the framework of Density Functional Theory (DFT), atomic structures and electronic properties of MoS₂/HfO₂ interface are investigated. The impact of interfacial oxygen concentration on the MoS₂/HfO₂ interface electronic structure is examined in order to mimic the atomic layer deposition growth at ambient conditions. Then, the effect on band offsets and the thermodynamic stability of those interfaces is investigated and compared with available relevant experimental data. These results seem to indicate that, for a well-prepared interface, the electronic device performance should be better than other interfaces like III-V/high-κ due to the absence of

interface defect states. However, any unpassivated defects, if present during oxide growth, strongly influence the subsequent electronic properties of the interface.

I.INTRODUCTION

For the development of future metal-oxide field effect transistors (MOSFETs), the conventional silicon (Si) transistor channel, which has already reached its physical limit of scaling, has to be replaced by an alternative material with higher carrier mobility,¹ and a high- κ dielectric providing higher gate capacitance for thicker films. For this purpose, III-V semiconductors have been studied extensively; they provide high electron and hole drift mobilities^{1, 2, 3}. Also, to be a suitable candidate for the use in future field effect devices, the material should be thermodynamically stable with the corresponding high- κ oxide and it also should be able to unpin the harmful Fermi level with minimal defect trap density (D_{it}). Many studies are focused on using hafnium dioxide (HfO_2) based dielectrics because of their high dielectric constant (≈ 20), thermal stability, and sufficient band offsets. Despite the enormous effort to realize a low D_{it} III-V/high- κ interface, these materials continue to suffer from high defect densities leading to threshold voltage shifts, large leakage current, and charge trapping, thus causing instability of the device. The nature and origin of those defects at the interface continues to be investigated in order to optimize the oxide growth deposition conditions and adopt a suitable defect passivation mechanism^{4, 5}.

Recently, there has been substantial interest on two dimensional (2D) materials (like graphene^{6, 7, 8}) for electronic device applications, due to their higher carrier mobilities and

interfaces devoid of defect states. However, due to the intrinsic zero band gap at the Dirac point, graphene based layered FETs suffer from high leakage currents. In addition, tuning the band gap of graphene is not feasible, which limits its potential applications^{9, 10}. Due to this, the semiconductor device community has turned the attention into other 2D or binary quasi-2D materials beyond graphene, because of their unique electronic, optical, chemical and mechanical properties for a wide range of future applications. Among these, transition metal dichalcogenides (TMDs), well known for being used as lubricant additives or coating because of their interesting tribological properties,^{11, 12, 13} have also attracted interest for device applications.

TMDs have a layered bulk structure which can be exfoliated into a single layer semiconducting 2D material with sizable band gaps or metallic behavior, depending on the type of metal-chalcogen combination¹⁴⁻²⁰. Ideally, these materials are anticipated to have a low D_{it} , as the dangling bond density should be minimal. They have been obtained by mechanical or chemical exfoliation as well as chemical vapor deposition techniques^{9, 21-25}. 2D MoS₂ has been recently investigated for electronic device applications, showing a promising performance of high ON-OFF current ratio (10^8), a carrier mobility of ~ 200 cm²/Vs⁹ and higher current density^{26, 27} with a high- κ gate dielectric. Using a scandium electrode, the carrier mobility can be further enhanced to ~ 700 cm²/Vs, suggesting a negligible Schottky barrier at MoS₂/Sc interface²⁸. Although initial reports show mobilities in the range of 0.1 to 10cm²/Vs for exfoliated monolayer MoS₂ on SiO₂⁶, a recent study claims a mobility enhancement by reducing the impurity scattering by high- κ deposition²⁹.

A recent study on quantum transport simulations of an idealized TMD device indicate that monolayer MoS₂ MOSFETs with HfO₂ can provide near-ideal subthreshold slope, suppression of drain-induced barrier lowering (DIBL), and gate-induced drain leakage³⁰. The switching behavior of a TMD transistor degrades significantly with thicker layers due to diminished gate control. Monolayer TMDs show the best scalability with the largest ON-OFF ratios, achieving ON current levels of 450 $\mu\text{A}/\mu\text{m}$ for an ON-OFF ratio of 10^5 while the bilayer devices deliver about half of this value exhibiting significant loss of gate control upon addition of an extra layer to the conducting channel³¹. Currently, a detailed investigation at the atomic level of the nature of TMD and high- κ dielectrics interface is still missing in the literature. For a detailed understanding and further optimization of the TMD based electronic devices, it is important to examine the detailed atomic and electronic structures of the TMD/HfO₂ interfaces under different growth conditions.

In this work, a lattice matched monolayer of MoS₂ and HfO₂ interface model is developed, and the interface atomic structures and the corresponding electronic properties are investigated using density functional theory (DFT) calculations at different levels of accuracy. The model interface was extensively investigated as a function of oxygen and hydrogen incorporation representing different HfO₂ Atomic Layer Deposition (ALD) growth conditions on MoS₂. The DFT results are compared with previously reported experimental values from *in situ* X-ray Photoelectron Spectroscopy (XPS) studies of HfO₂ ALD on bulk MoS₂³². Moreover, we also investigate the influence of several

structural defects and disorders at the interface on the electronic properties. These studies on MoS₂/HfO₂ can be extended to other TMDs and high- κ oxides in an effort to identify the most promising device material candidate which might improve the performance of MoS₂.

The organization of this paper is as follows. Computational methods are presented in Section II, the results and discussions of our findings are presented in Section III. Finally, summary of the findings are presented on section IV.

II. COMPUTATIONAL METHODS

First-principles calculations based on Density Functional Theory (DFT)³³⁻³⁵ with plane wave basis set and Projector Augmented Wave (PAW) pseudopotentials³⁶⁻³⁷ implemented in the Vienna *Ab-initio* Simulation Package (VASP)^{33, 38} have been carried out. The electronic wave functions are represented by plane wave basis with a cutoff energy of 500 eV. The exchange correlation interactions are incorporated as a functional of Generalized Gradient Approximation (GGA)^{39, 40}. Knowing the underestimation of the band gaps obtained from standard GGA calculations, we also used the hybrid functional proposed by Heyd, Scuseria, and Ernzerhof (HSE)⁴¹ in which the short-range part of the exchange functional is represented by a (fixed) combination of GGA- and Hartree-Fock contributions, while the long-range part and the correlation functional are described by the GGA.

In order to investigate the MoS₂/HfO₂ interface, an interface model starting with a S terminated MoS₂ surface and O terminated HfO₂ (111) surface with a lattice mismatch

less than 1% is constructed, as shown in Fig. 1(a). This interface model contains 5 atomic layers of Hf and 10 atomic layers of O to minimize the quantum size effects. Periodically repeated slabs are used to model the interface. Each periodic slab is separated by 16 Å of vacuum to avoid interaction between the two surfaces of the slab as a result of the periodic boundary conditions. In our calculations, the atoms are allowed to relax while the cell size is kept fixed after optimization of the unit cell.

A Γ -centered $6\times 6\times 1$ k-point mesh is used in the self-consistent field (SCF) calculations and a $12\times 12\times 1$ k-point mesh is used for density of states (DOS) calculations. A SCF dipole correction is used to cancel spurious electric fields that may be induced by the periodic boundary conditions of the interface model. The energy and forces are converged until a tolerance value of 10^{-4} eV and 0.01 eV/Å, respectively. In our model, the interface area is 33.99 Å² with a strain of 0.58 % and the lattice vectors form an angle of 60° , as it can be seen in Fig. 1(b).

III. RESULTS AND DISCUSSION

A. Pristine interface

First, we optimized the atomic structure of the stoichiometric $\text{MoS}_2/\text{HfO}_2$ interface model and analyzed its electronic structure. Then, the oxygen concentration at the interface is varied in order to investigate the impact on the electronic properties of the interface. Figure 2(a) shows the electrostatic potential variation across a direction perpendicular to the interface area of the model. The vacuum level is flat, indicating that

there is no electrostatic polarization (no significant charge transfer) caused by HfO₂ deposition on the MoS₂ layer. This fact indicates that there is a very weak van der Waals interaction between the MoS₂ monolayer and the HfO₂. This is consistent with a recent experimental study on ALD of HfO₂ on the MoS₂ surface that did not detect any covalent bonding between the HfO₂ and MoS₂ layers³². Symmetric potential profiles are observed for the MoS₂ monolayer and HfO₂. The overlap between the MoS₂ interface and the isolated MoS₂ potentials indicates that there is no chemical bonding or charge transfer across the interface.

In order to understand the electronic properties and to obtain the band offsets (BOs) between MoS₂ and HfO₂ across the interface, the local density of states (LDOS) at bulk-like Hf, O, Mo and S atoms away from interface is computed. The LDOS is shown in Fig. 2(b), as obtained from GGA calculations. The computed band gaps of HfO₂ are 4 eV and 6 eV, as obtained with GGA and HSE, respectively (*cf.* with the experimental result of 5.9 eV³²). For the MoS₂/HfO₂ interface, GGA calculations yield a band gap of 1.8 eV, whereas HSE results widen the gap to 2.34 eV. Then, even though the HSE band gap of HfO₂ matches the experimental result much better than the GGA, the qualitatively band offsets of the interface remains relatively unchanged.

Valence Band Offset (VBO) and Conduction Band Offset (CBO) obtained from GGA calculations are ≈ 1.0 eV and ≈ 1.24 eV respectively, whereas HSE calculations yield a CBO of ≈ 2.0 eV and a VBO of ≈ 1.60 eV. The corresponding experimental values for the bulk interface are CBO ≈ 2.09 eV and VBO ≈ 2.67 eV ($E_g = 1.23$ eV (bulk)³²).

These results show that, qualitatively and quantitatively, the BOs are sufficient to avoid the leakage current during electronic device operation, even though the calculations of the BOs are for a single MoS₂ monolayer; whereas the available experimental values were obtained for the bulk MoS₂ and HfO₂ interface.

B. Interfacial oxygen concentration

In order to mimic the oxidizing environment of the ALD process and to model the experimental conditions in a more realistic manner, the interfacial oxygen concentration is varied and the effect on the corresponding electronic properties is investigated. Our calculations show strong effects of the interfacial oxygen content on the electronic structure of the interface and the corresponding BOs.

Figure 3 shows the atomic structures of the MoS₂/HfO₂ interface at several levels of oxygen concentration (O6 refers to six interfacial O atoms, corresponding to a high oxygen concentration (1.76×10^{15} O atoms/cm²), and O3 refers to the lower limit of three interfacial O atoms (0.88×10^{15} O atoms/cm²) within the unit cell of the interface model). Then, the electronic band structures of those interfaces are investigated to elucidate the impact of the oxygen concentration on the properties of the interface. Figure 3 (a) -3(d) show the band structures of the MoS₂/HfO₂ interface with different oxygen concentrations at the interface and Table I summarizes our obtained results. The O6 model shows an indirect band gap with values of $E_g = 1.00$ eV (GGA) and 1.59 eV (HSE), O5 band gap is also of indirect type: 1.43 eV (GGA) and 2.28 eV (HSE). On the

contrary, the band gaps of the O4 and O3 models are of direct type, and their obtained values are 1.83 eV (GGA) and 2.37 eV (HSE) for the O4 model and 1.84 eV (GGA) and 2.34 eV (HSE) for the O3 model (see Table I).

For device applications, the evaluation of the BOs between MoS₂ and HfO₂ as a function of the oxygen concentration is very important, as the BOs are one of the key parameters that reflect the quantum mechanical electron tunneling mechanism across the interface. From the analysis of the variation of the potential across the interface in the previous section, there is no significant charge transfer for the stoichiometric interface. In the absence of charge transfer, the BOs are obtained by the electron affinity (EA) rule or Anderson's rule⁴². In our model, the change of the interfacial oxygen concentration directly affects the EA. It is observed that the VBO is at least 1 eV (1.8 eV) for the O3 model in the GGA (HSE) level of approximation and, also, the BOs increase with the amount of O concentration at the interface (see Table I).

The LDOS of bulk-like Hf, O, Mo and S atoms in MoS₂ and HfO₂ far away from the interface region are computed, to find the energy difference between their valence band maxima (VBM). Then, the CBO can be obtained by using the experimental band gaps of MoS₂ and HfO₂ in order to avoid the influence of GGA band gap underestimation. The change in the O concentration at the interface affects the states of HfO₂, not those of the MoS₂, since the VBM of HfO₂ is dominated by O 2*p* states. Higher O concentration shifts down the VB edge of HfO₂ due to the O 2*p* re-distribution at the VBM. As a consequence, the VBO increases with the amount of interfacial oxygen. Thus, the VBO

can be controlled by varying the oxygen concentration, a property directly related to the ambient atmospheric oxygen pressure during the oxide formation.

By controlling the interfacial O concentration gradually, the VBOs can be modified up to 1.8 eV (O3=1.0 eV, O4=1.8 eV, O5=2.3 eV and O6=2.8 eV) at the GGA level of calculation. Figure 6 shows the LDOS obtained using the HSE hybrid functional. The results show that the VBO can be altered up to 2.3 eV by controlling the oxygen concentration. However, significant reduction of the CBO is seen for higher oxygen concentrations (see Fig.4). This variation of the BOs will significantly affect any device performance. However, the trend showing a band gap narrowing with the increase of oxygen concentration remains unchanged. Our obtained results are comparable to the previously reported experimental value for the bulk MoS₂/ HfO₂ system³².

C. Hydrogen incorporation at the interface

Apart from oxygen, hydrogen impurities strongly alter the structural and electronic properties of different host materials into which they are incorporated, impacting the performance of the electronic devices. During ALD growth process, the use of water as an oxygen precursor can provide hydrogen species in the semiconductor surface. Defect (dangling bond) passivating effects or dopant passivation behavior are well known in conventional semiconductors. In the present work, the presence of H atoms at the interface at several oxygen concentrations is examined (see Fig. 5). Figure 5(a)-5(f) shows the band structures and Fig. 6 the LDOS of the different configurations

considered. The notation O_x-yH refers to the interface with x number of O atoms and y number of H at the interface. The obtained results show that, for the O3 model, the additional H atom results in n -type doping behavior, as it can be seen from the shifting of the Fermi level up to the conduction band in the band structure diagram shown in Fig. 5 (a). However, for the O6 model, the H impurity forms an OH bond, inducing defect states close to the Fermi level. Then, both H and OH at the interface show a strong impact on the electronic properties of the interface. Additionally, OH like species present at the interface shift the Fermi level towards the valance band edge and exhibit p -type doping behavior and gap states (which can be potentially harmful for device applications), as observed in Figs. 5(e) and 5(f). It is worthwhile to note that OH species are expected to be in abundance in a standard deposition process, such as ALD. We noted that the incorporation of a H impurity (0.88×10^{15} H atoms/cm²) on the stoichiometric interface model causes a defect state density around (1.5×10^{14} /cm² eV) close to the band edges.

D. Interface and disorder

Structural disorder at the interface originated during the growth process also affects the electronic properties and the thermodynamic stability of the resulting device. We will examine the thermodynamic stability in the next Section. In this section, we propose several possible defective interfaces (see Fig. 7) to see how the electronic properties are affected by a different atomic arrangement. The notation O6-O-S refers to the interface with modified O6 model in which O from HfO₂ are interchanged with S from MoS₂ side

as shown in Fig. 7(a), along with the corresponding electronic band structures exhibiting additional bands inside the band gap of MoS₂. The notation O7-O-S refers to the interface where bottom sulfurs of MoS₂ are completely replaced by O atoms and interfacial O atoms of the HfO₂ are bonded with S atoms, as shown in Fig. 7(b). It can be seen that these interchange defects are causing interface defect states in the band gap of MoS₂ between 1.2 and 1.5×10^{-4} eV cm², for a defect density around 1×10^{15} O or H atoms/cm².

Defect state generation can be anticipated if there is S and O bonding at the interface. S and O interchange to form Mo-O and S-O bonds strongly reduces the band gap and the defect states. In pristine MoS₂, VBM contribution is from the hybridization of Mo *d* orbital and S *p* orbital, whereas CBM is mainly composed of Mo *d* orbitals. In the disordered interface, the hybridization is weakened due to re-hybridization at the interface, inducing gap states in the band gap of MoS₂. Thus, if those extrinsic defects are present at the interface, gap states will be induced, resulting in a deleterious impact on device behavior. The band structure shown in Fig. 7(c) of a S-Mo-O layer with HfO₂ shows that the band gap narrows substantially showing a metallic character (MoO₂ is metallic⁴³). This study also indicates the possibility of utilizing such interface to make contact materials due to the metallic nature of the contact for future TMD devices⁴⁴.

E. Thermodynamic stability of the various interface model

In order to determine the thermodynamic stability of the different interface models, we investigate their formation energies. The ground state of the MoS₂/HfO₂

interface is determined by minimizing the thermodynamic potential. The relative stability of the different interface models is then obtained by comparing their formation energies, given by:

$$E^{form} = \frac{E_{tot} - n E_{Hf} - m E_S - k E_{Mo} - l \mu_O - p \mu_H}{A} \quad (1)$$

where E^{form} is the interface formation energy, E_{tot} is the total energy of the system, A is the total interfacing area of the slab, μ_i are the chemical potentials for the respective elements and n , m , k , l and p are the number of Hf, S, Mo, O and H atoms. The total energy (DFT) is used here (instead of the Gibb's free energy) for the calculations of the formation energies since the entropy contributions and enthalpy changes due to finite temperature are insignificant for all the structures resulting in an insignificant change in the relative interface formation⁴⁵.

The energy of bulk HfO₂ and MoS₂ can be written in terms of the gas phase reaction of an oxygen molecule and the Hafnium metal and bulk Mo and S and their respective heats of formation:

$$\begin{aligned} E_{HfO_2}(bulk) &= E_{Hf}(bulk) + \mu_{O_2}(bulk) + \Delta H_{HfO_2}^f \\ E_{MoS_2}(bulk) &= E_{Mo}(bulk) + 2\mu_S(bulk) + \Delta H_{MoS_2}^f \end{aligned} \quad (2)$$

Using equation (2) and setting the oxygen gas phase as a reference, the numerator of equation (1) can be re-written as follows:

$$\begin{aligned} E^{form} &= E_{tot} - [n (E_{HfO_2}(bulk) - \mu_{O_2}(bulk) - \Delta H_{HfO_2}^f) + m E_S \\ &\quad + k (E_{MoS_2}(bulk) - 2\mu_S(bulk) - \Delta H_{MoS_2}^f)] - l \mu_O - p \mu_H \end{aligned} \quad (3)$$

Now , one can rearrange this equation to obtain the interface formation energy per unit area,

$$E^{form} = \frac{E_{tot} - nE_{HfO_2}(bulk) - kE_{MoS_2}(bulk) + n\Delta H_{HfO_2}^f + k\Delta H_{MoS_2}^f + (2n - l)\mu_O + (2k - m)\mu_S - p\mu_H}{A} \quad (4)$$

With the restriction of the chemical potential of oxygen and Hf,

$$\mu_O \leq \mu_O(bulk) = \frac{1}{2} E_{O_2} \text{ and } \mu_{Hf} \leq \mu_{Hf}(bulk) = E_{Hf} \quad (5)$$

The thermodynamic range of oxygen chemical potential for the interface model can then be obtained:

$$\frac{1}{2} (E_{O_2} + \Delta H^f) \leq \mu_O \leq \frac{1}{2} E_{O_2} \text{ which results in } -10.39 \text{ eV} \leq \mu_O \leq -5.01 \text{ eV}.$$

(6)

The interface formation energy as a function of oxygen chemical potential (μ_o) is shown in Fig. 8. The right hand side corresponds to the O-rich limit (*i.e.*, the μ_o is set to zero) whereas the left hand side of the plot represents the O-poor limit. The formation energy increases gradually when oxygen chemical potential changes from O-rich limit to the O-poor limit for O₆ to O₃ interface models, with the oxygen rich environment being thermodynamically favorable. Similar behavior is seen in III-V and high- κ interfaces^{46, 47, 48}. To compare our results with a realistic ALD oxide growth condition of HfO₂ on MoS₂ at 600K, we correlate the chemical potential with the oxygen partial pressure using the following equation (plotted on the top axis of the Fig. 8):

$$\mu_0(T, P) = \mu_0(T, P^0) + \frac{1}{2} k T \ln\left(\frac{P}{P^0}\right) \quad (7)$$

where, P and P^0 are the pressures at T temperature and at one atmosphere, respectively.

Figure 8 shows that the thermodynamic stability of the O3 model is higher than that of O4, O5 and O6 models for a wide range of chemical potentials, albeit far from realistic ALD conditions. The relative formation energy of the O6-3H defect model is relatively low in the range close to a partial pressure of 1 atm, showing that it is stable in O rich environments. The stability of the O3-H model is lower than that of the O3 model, showing that for a stoichiometric interface, H impurities increase the formation energy. However, the O7-O-S model is the least stable among all the interface models investigated, but O7-O is stable in O-rich conditions. This thermodynamic analysis indicates that most of the defective surfaces are less likely to be formed. But, on the contrary, additional hydrogen impurities at the interface are more likely to be formed compared to the stoichiometric MoS₂/HfO₂ interface (O3 model).

IV. SUMMARY

Using first-principles calculations based on DFT, we studied several MoS₂/HfO₂ interface models, in order to investigate the atomic and electronic properties of the ideal interface and under different ALD growth conditions. Our results show that the stoichiometric MoS₂/HfO₂ interface is devoid of any defect states in the fundamental band gap of MoS₂, indicating a superior performance than that of the III-V/HfO₂

interfaces in terms of no induced defect states for a pristine MoS₂ monolayer. We observed that the BOs change as interfacial O content increases, indicating their dependence on the oxide growth environment. For the stoichiometric MoS₂/HfO₂ interface without any defects at the interface, no charge transfer between HfO₂ and MoS₂ is observed. However, disorder and defects at the interface can introduce gap states, which would be harmful for device applications due to subsequent charge transfer. Thus, the interfacial oxygen content strongly affects the thermodynamic stability and the BOs of the interface. Furthermore, interfacial hydrogen impurities are also shown to have strong influence on the interfacial stability and the corresponding VBO. These DFT results of MoS₂/HfO₂ interface properties are qualitatively consistent with those obtained from *in situ* XPS studies of HfO₂ ALD on bulk MoS₂.

ACKNOWLEDGEMENTS

We would like to thank all the members associated in LEAST at UTD for their fruitful discussions, in particular Prof. Christopher Hinkle, Dr. Luigi Colombo, Dr. Stephen McDonnell and Ms. Angelica Azcatl. RMW acknowledges discussions with Prof. A. Javey on contact interfaces. This work was supported in part by the Center for Low Energy Systems Technology (LEAST), one of six centers supported by the STARnet phase of the Focus Center Research Program (FCRP), a Semiconductor Research Corporation program sponsored by MARCO and DARPA. All the calculations were performed using computational resources of Texas Advanced Computer Center (TACC) at University of Texas at Austin.

REFERENCES

- 1 J. A. del Alamo, *Nature* **479**, 317 (2011).
- 2 See: *Fundamentals of III-V Semiconductor MOSFETs*, edited by S. Oktyabrsky and P. D. Ye (Springer, New York, 2010), and references therein.
- 3 H. Hasegawa, *Jpn. J. Appl. Phys.* **38**, 1098 (1999).
- 4 C. J. Sandroff, R. N. Nottenberg, J. C. Bischoff, and R. Bhat, *Appl. Phys. Lett.* **51**, 33 (1987).
- 5 C. J. Sandroff, M. S. Hegde, L. A. Farrow, C. C. Chang, and J. P. Harbison, *Appl. Phys. Lett.* **54**, 362 (1989).
- 6 K. S. Novoselov, A. K. Geim, S. V. Morozov, D. Jiang, Y. Zhang, S. V. Dubonos, I. V. Grigorieva, and A. A. Firsov, *Science* **306**, 666- 669 (2004).
- 7 X. Li, W. Cai, J. An, S. Kim, J. Nah, D. Yang, R. Piner, A. Velamakanni, I. Jung, and E. Tutuc, *Science* **324**, 1312-1314 (2009).
- 8 A. Reina, X. Jia, J. Ho, D. Nezich, H. Son, V. Bulovic, and M. S. Dresselhaus, J. Kong, *Nano Lett.* **9**, 30-35 (2008).
- 9 B. Radisavljevic, A. Radenovic, J. Brivio, V. Giacometti, and A. Kis, *Nat. Nanotech.* **6**, 147-150 (2011).
- 10 S. Zhou, G.-H. Gweon, A. Fedorov, P. First, W. De Heer, D.-H. Lee, F. Guinea, A. C. Neto, and A. Lanzara, *Nat. Mater.* **6**, 770-775 (2007).
- 11 L. Rapoport, N. Fleischer, and R. Tenne, *Adv. Mater.* **15**, 651 (2003).
- 12 S. Brown, J. L. Musfeldt, I. Mihut, J. B. Betts, A. Migliori, A. Zak, and R. Tenne,

- Nano Lett.* **7**, 2365 (2007).
- 13 T. Onodera *et al.*, *J. Phys. Chem. B* **113**, 16526 (2009).
 - 14 Y. Ding, Y. Wang, J. Ni, L. Shi, S. Shi, and W. Tang, *Physica B*, **406**, 2254 (2011).
 - 15 A. Ayari, E. Cobas, O. Ogundadegbe, and M. S. Fuhrer, *J. Appl. Phys.* **101**, 014507 (2007).
 - 16 E. Morosan, H. W. Zandbergen, B. S. Dennis, J. W. G. Bos Y. Onose, T. Klimczuk, A. P. Ramirez, N. P. Ong, and R. J. Cava, *Nat. Phys.* **2**, 544 (2006).
 - 17 W. Z. Hu, G. Li, J. Yan, H. H. Wen, G. Wu, X. H. Chen, and N. L. Wang, *Phys. Rev. B* **76**, 045103 (2007).
 - 18 A. F. Kusmartseva, A. Akrap, H. Berger, L. Forro, and E. Tutis, *Nat. Mater.* **7**, 960 (2008).
 - 19 K. K. Kam, and B. A. Parkinson, *J. Phys. Chem.* **86**, 463 (1982).
 - 20 S. W. Han, H. Kwon, S. K. Kim, S. Ryu, W. S. Yun, D. H. Kim, J. H. Hwang, J.-S. Kang, J. Baik, H. J. Shin, and S. C. Hong, *Phys. Rev. B* **84**, 045409 (2011).
 - 21 K. S. Novoselov, D. Jiang, F. Schedin, T. J. Booth, V. V. Khotkevich, S. V. Morozov, and A. K. Geim, *Proc. Natl. Acad. Sci. USA* **102**, 10451 (2005).
 - 22 J. N. Coleman *et al.*, *Science* **331**, 568 (2011).
 - 23 Y. Shi, W. Zhou, A.-Y. Lu, W. Fang, Y.-H. Lee, A. L. Hsu, S. M. Kim, K. K. Kim, H. Y. Yang, L.-J. Li, J.-C. Idrobo, and J. Kong, *Nano Lett.* **12**, 2784 (2012).
 - 24 Y. Zhan, Z. Liu, S. Najmaei, P.M. Ajayan, and J. Lou, *Small* **8**, 966 (2012).
 - 25 G. Eda, H. Yamaguchi, D. Voiry, T. Fujita, and M. Chen, *Nano Lett.* **11**, 5111 (2011).
 - 26 L. Liu, S. Kumar, Y. Ouyang, and J. Guo, *IEEE T. Electron Dev.* **58**, 3042 (2011).

- 27 Y. Yoon, K. Ganapathi, and S. Salahuddin, *Nano Lett.* **11**, 3768 (2011).
- 28 S. Das, H.-Y. Chen, A.V. Penumatcha, and J. Appenzeller, *Nano Lett.* **13**, 100-105 (2013).
- 29 D. Jena, and A. Konar, *Phys. Rev. Lett.* **98**, 136805, (2007).
- 30 J. Chang, L. F. Register, and S. K. Banerjee, *Appl. Phys. Lett.* **103**, 223509 (2013).
- 31 V. Mishra, S. Smith, K. Ganapathi and S. Salahuddin, *IEEE Electron Devices Meeting (IEDM) Technical Digest*, 139 (2013). DOI: 10.1109/IEDM.2013.6724569
- 32 S. McDonnell, B. Brennan, A. Azcatl, N. Lu, H. Dong, C. Buie, J. Kim, C. L. Hinkle, M. J. Kim, and R. M. Wallace, *ACS Nano* **7** (11), 10354 (2013).
- 33 G. Kresse, and J. Furthmuller, *J. Comput. Mater. Sci.* **6** (1)15-50, (1996).
- 34 R. G. Parr and W. Yang, *Density-Functional Theory of Atoms and Molecules* Oxford University Press, New York, (1989).
- 35 W. Kohn, and L. J. Sham, *Phys. Rev.* **140**, A1133 (1965).
- 36 G. Kresse, and D. Joubert, *Phys. Rev. B* **59**, 1758 (1999).
- 37 P. E. Blochl, *Phys. Rev. B* **50**, 17953 (1994).
- 38 G. Kresse, and J. Hafner, *Phys. Rev. B* **47**, 558 (1993).
- 39 G. Kresse, and J. Furthmuller, *Phys. Rev. B* **54**, 11169 (1996).
- 40 G. Kresse, and J. Hafner, *Phys. Rev. B* **49**, 14251 (1994).
- 41 J. Heyd, G. E. Scuseria, and M. Ernzerhof, *J. Chem. Phys.* **118**, 8207 (2003), *J. Chem. Phys.* **124**, 219906 (2006).
- 42 R. L. Anderson, *IBM J. Res. Dev.* **4**(3), pp. 283-287 (1960).
- 43 P. Thakur, J. C. Cezar, N. B. Brookes, R. J. Choudhary, R. Prakash, D. M. Phase, K.

- H. Chae, and R. Kumar , *Appl. Phys. Lett.* **94**, 062501 (2009).
- 44 S. Chuang, C. Battaglia, A. Azcatl, S. McDonnell, H. Fang, L. Kang, X. Yin, M. Tosun, R. Kapadia, R. M. Wallace, and A. Javey, (2013) (submitted).
- 45 J. Baik, H. J. Shin, and S. C. Hong, *Phys. Rev. B* **84**, 045409 (2011).
- 46 S. KC, H. Dong, W. Wang, R. C. Longo, K. Xiong, R. M. Wallace, and K. Cho, *J. Appl. Phys.* **115**, 023703 (2014).
- 47 K. Xiong, W. Wang, D. M. Zhernokletov, S. KC., R. C. Longo, R. M. Wallace, and K. Cho, *Appl. Phys. Lett.* **102**, 022901 (2013).
- 48 W. Wang, K. Xiong, R. M. Wallace, and K. Cho, *J. Phys. Chem. C*, **114** (51), 22610-22618 (2010).

Table and figure captions:

TABLE I: Band offsets between MoS₂ and HfO₂ for various interfacial oxygen concentrations.

Figure 1. Atomic structure of MoS₂/HfO₂ interface a) side view, b) top view. Hafnium, oxygen, molybdenum and sulfur are represented by *turquoise*, red, purple and yellow spheres, respectively.

Figure 2. (a) Electrostatic potential profile perpendicular to the interface area (along z-direction). The red lines represent the interfacial potential variation whereas the green line shows the isolated MoS₂ monolayer contribution. Both potentials are measured with respect to the E_{VBM}. **(b)** Band offsets from local density of states (LDOS) approach from GGA functional. The zero of the energy is aligned to the Fermi level.

Figure 3. (Left) Electronic band structures of MoS₂/HfO₂ interfaces with various oxygen concentrations at the interface. The zero of the energy is aligned to the Fermi level. (Right) Atomic structure of MoS₂/HfO₂ interfaces with various oxygen contents at the interface. Hafnium, oxygen, molybdenum and sulfur are represented by *turquoise*, red, purple and yellow spheres, respectively.

Figure 4. Estimation of the band offsets from local density of states (LDOS) approach, as obtained from HSE calculations. The zero of the energy is aligned to the Fermi level.

Figure 5. (Left) Electronic band structures of MoS₂/HfO₂ interface with H with OH bonding at the interface with low and high oxygen concentrations. The zero of the energy is aligned to the Fermi level. (Right) Atomic structure of the MoS₂/HfO₂ interfaces for several interfacial hydrogen concentrations. Hafnium, oxygen, molybdenum and sulfur are represented by *turquoise*, red, purple and yellow spheres, respectively (H impurities at the interface result in OH bonding).

Figure 6. Estimation of band offsets from local density of states (LDOS) for the MoS₂/HfO₂ interface with H defect incorporation to the O6 model, as obtained from HSE calculations. The zero of the energy is aligned to the Fermi level.

Figure 7. (Left) Electronic band structures of the MoS₂/HfO₂ system with several S-O defects at the interface (see text for details). The zero of the energy is aligned to the Fermi level. (Right) Corresponding atomic structures of the MoS₂/HfO₂ interfaces with S-O defects. Hafnium, oxygen, molybdenum and sulfur are represented by *turquoise*, red, purple and yellow spheres, respectively

Figure 8. Thermodynamic stability of the MoS₂/HfO₂ system for several oxygen, hydrogen and defect concentrations at the interface. The interface formation energy is given with respect to the oxygen chemical potential in the following range: $-5.38 \text{ eV} \leq \mu_{\text{O}} \leq 0 \text{ eV}$ (setting the bulk value to zero). The right plot is a zoom of the section corresponding to experimental conditions around 1 atm.

Table:

TABLE I.

Interface Model	Concentration (#O atoms/cm ²)	VBO (GGA) (eV)	VBO (HSE) (eV)	E _g (GGA) (eV)	E _g (HSE) (eV)
O ₃	0.88×10 ¹⁵	1.0	1.8	1.84	2.34
O ₄	1.18×10 ¹⁵	1.8	2.6	1.83	2.37
O ₅	1.48×10 ¹⁵	2.3	3.2	1.43	2.28
O ₆	1.76×10 ¹⁵	2.8	4.1	1.0	1.59

Figures:

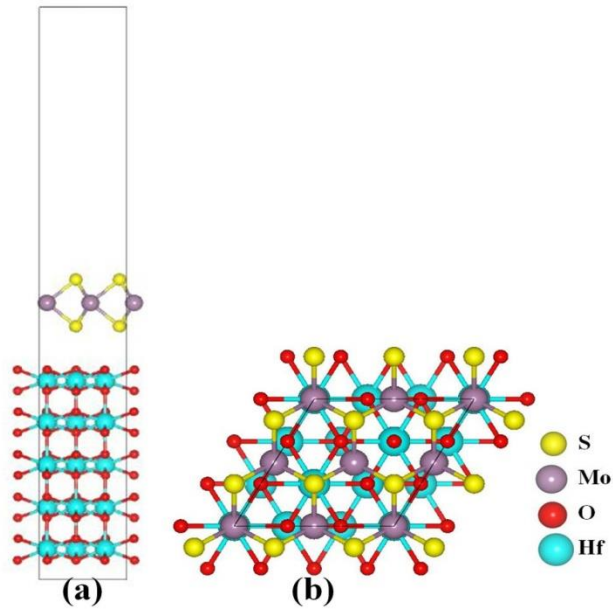


Figure 1.

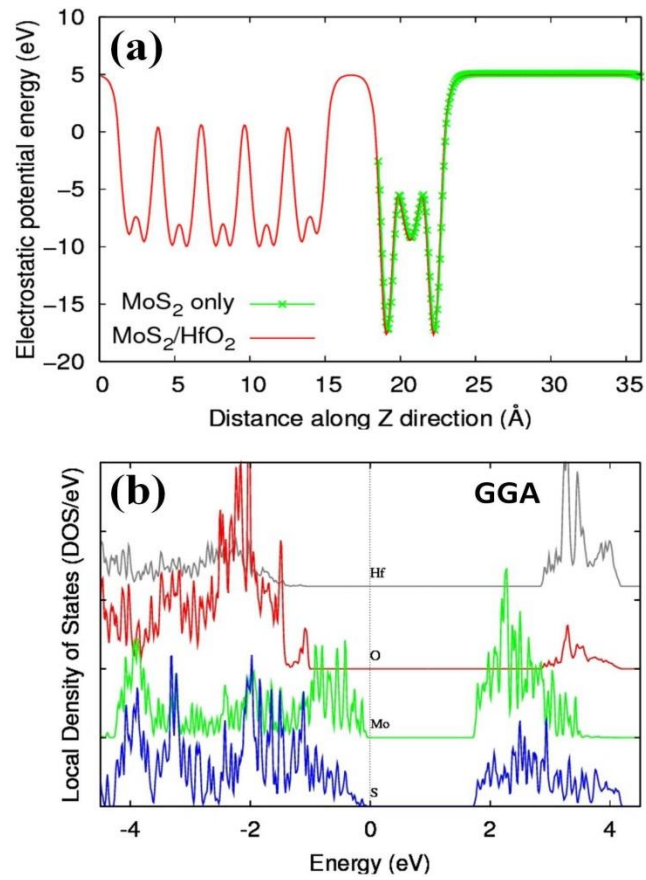


Figure 2.

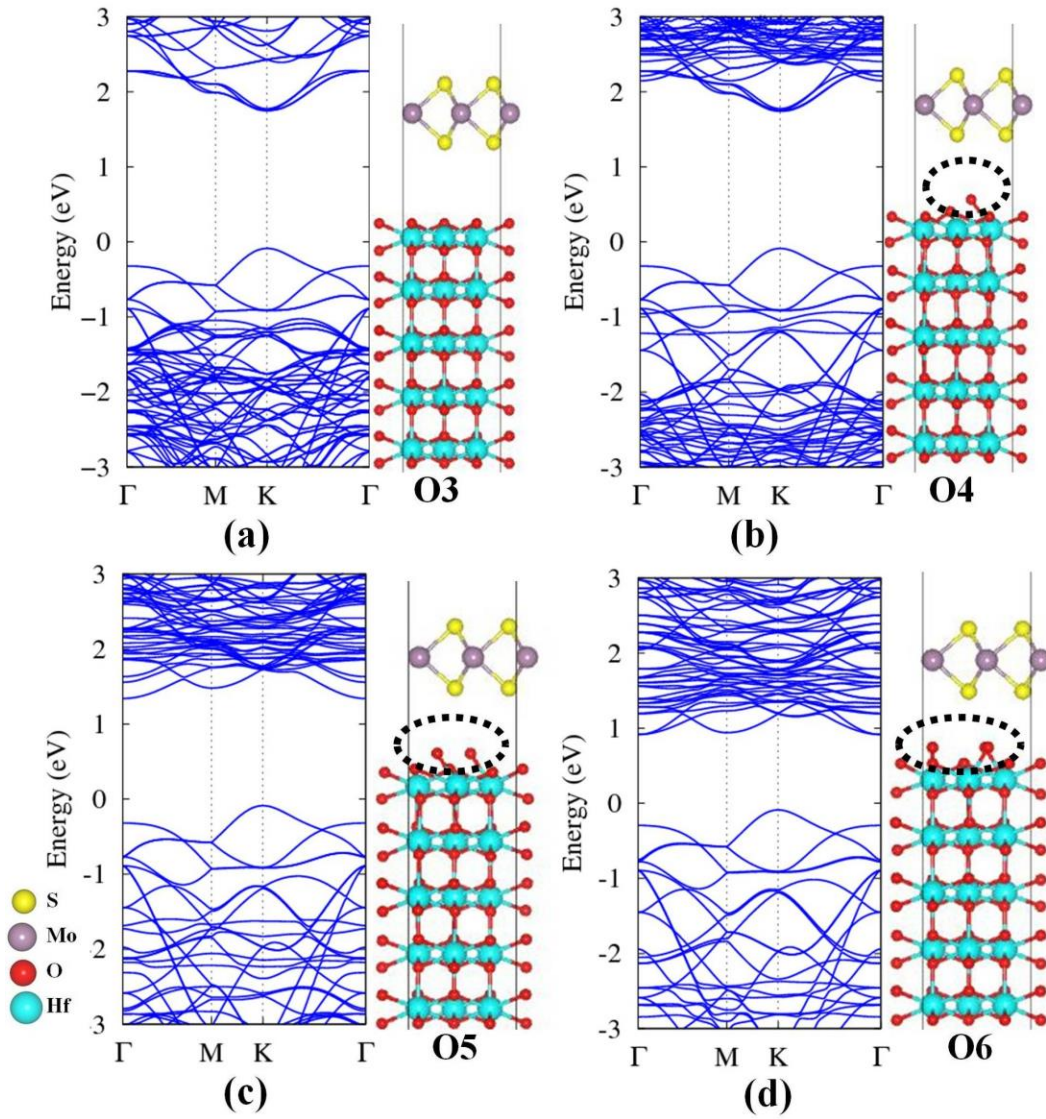


Figure 3.

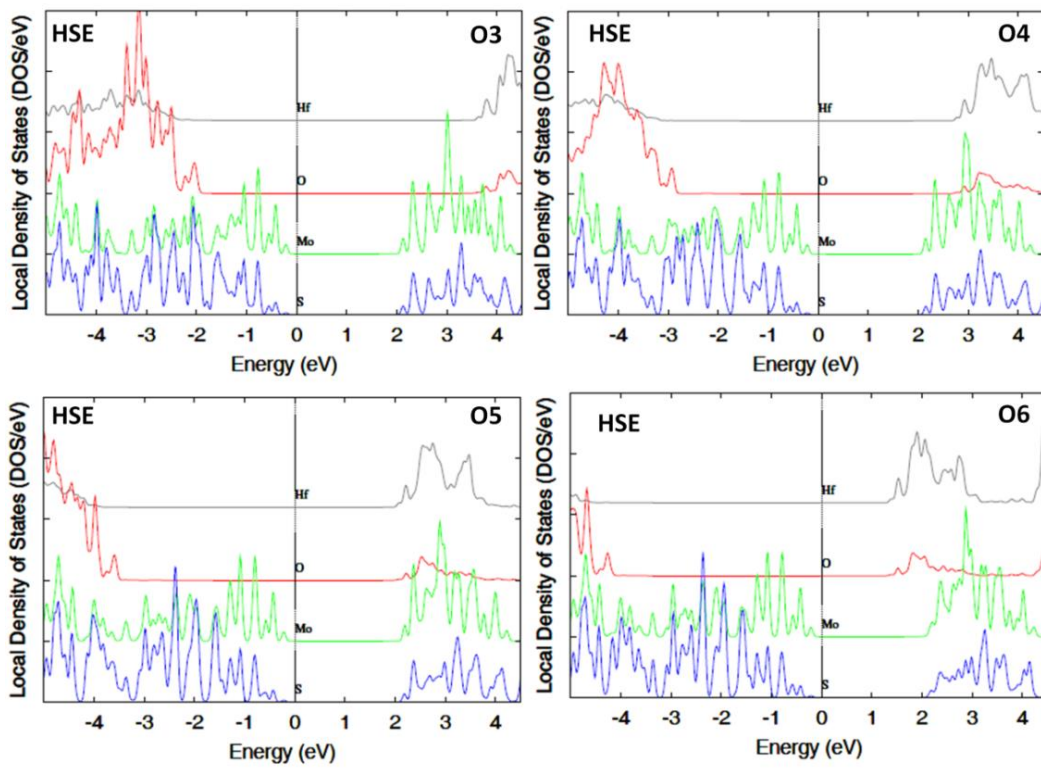


Figure 4.

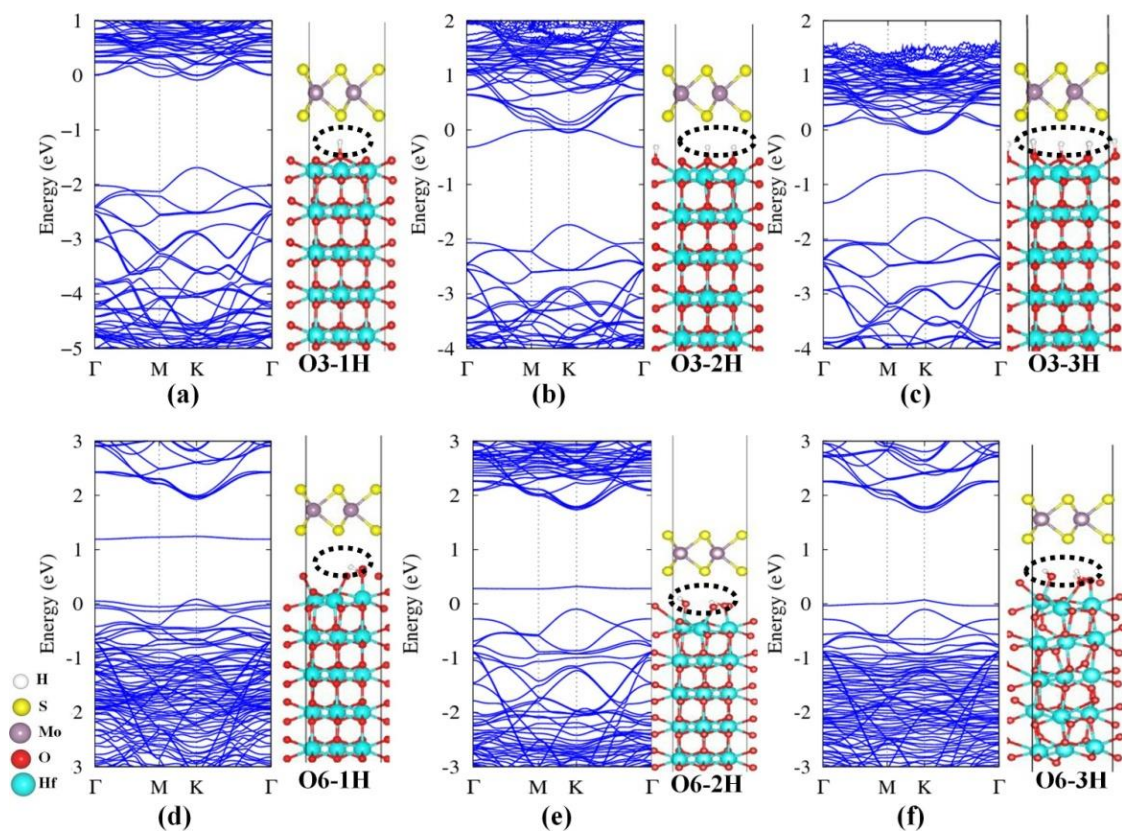


Figure 5.

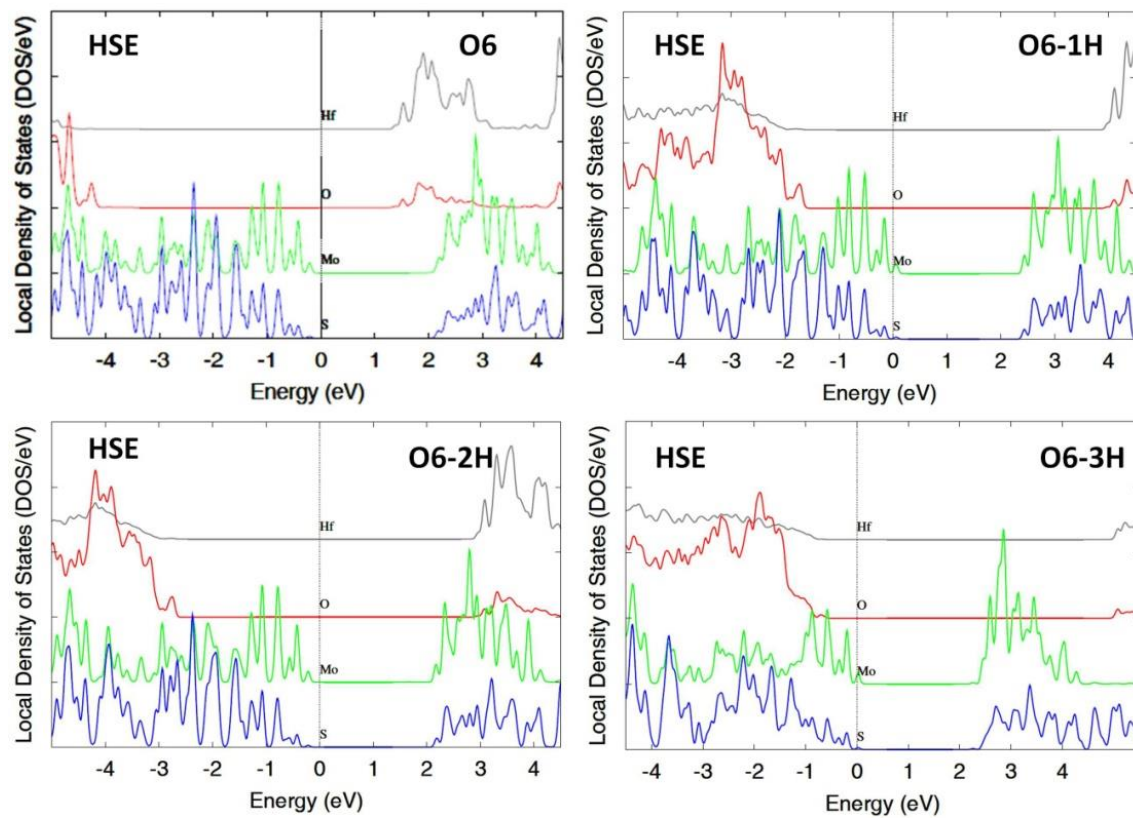


Figure 6.

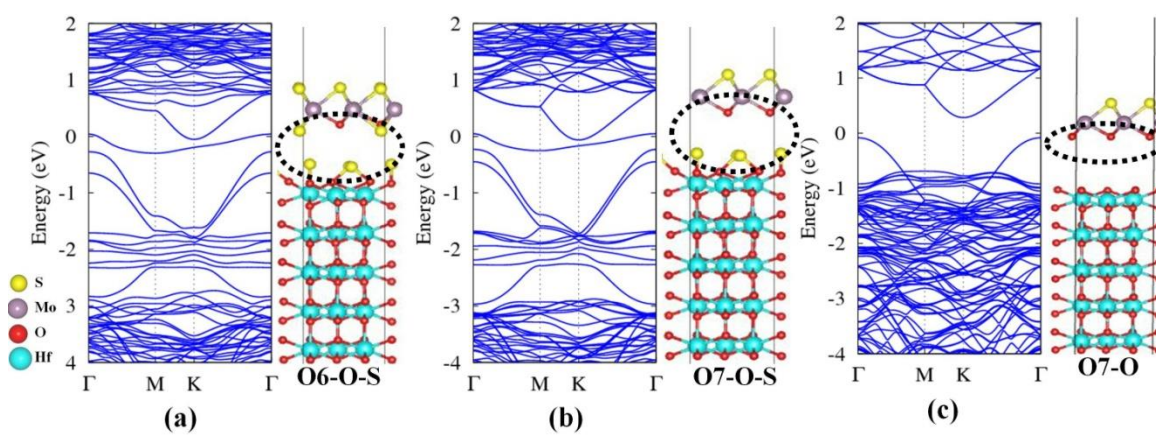


Figure 7.

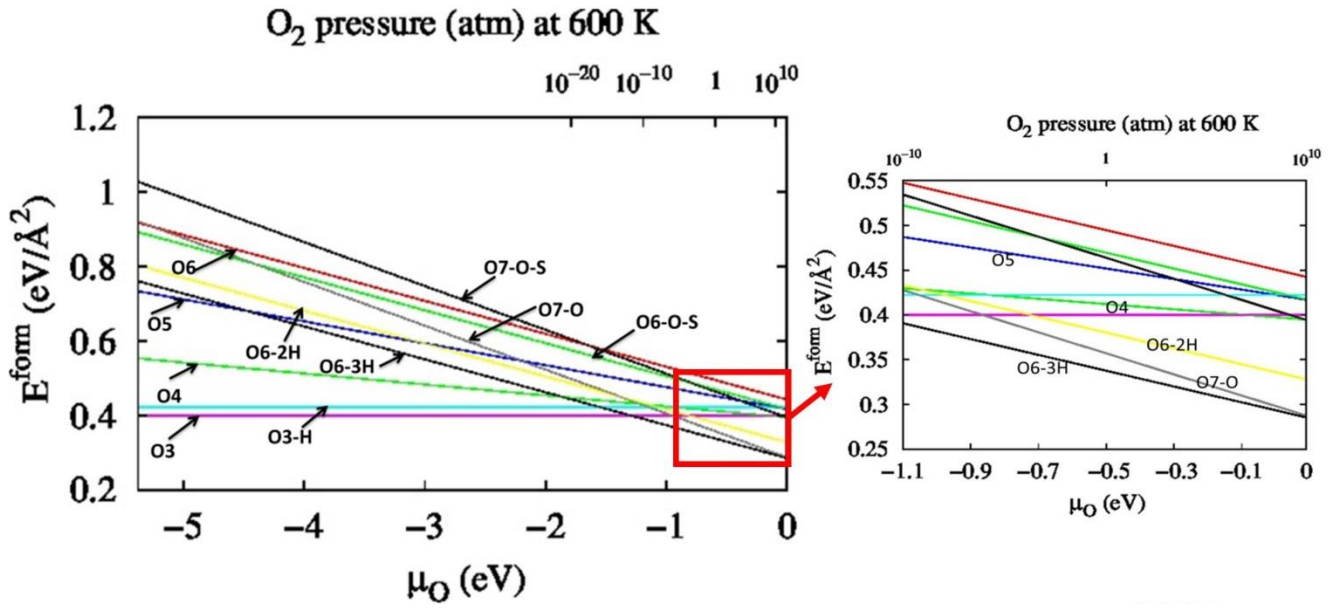


Figure 8.